Analyzing halftone dot blurring by extended spectral prediction models

Mathieu Hébert* and Roger David Hersch

Ecole Polytechnique Fédérale de Lausanne (EPFL), School of Computer and Communication Sciences, 1015 Lausanne, Switzerland

**Corresponding author: mathieu.hebert@univ-st-etienne.fr*

Received March 18, 2009; revised September 10, 2009; accepted November 5, 2009; posted November 5, 2009 (Doc. ID 108914); published December 3, 2009

Spectral prediction models for halftone prints generally assume homogeneously thick and sharply edged ink dots, i.e., bilevel halftones. In real prints, the ink thickness often decreases at the boundaries of the ink dots, thereby forming continuous-level halftones. The present study aims at verifying to what extent the classical Clapper–Yule and Yule–Nielsen models are able to predict the reflectance of single-ink continuous-level halftone prints. First we model the reflectance of continuous-level halftones by developing variable thickness extensions of both the Clapper–Yule and the Yule–Nielsen spectral prediction models. We consider continuous halftones whose thickness profiles are obtained by Gaussian filtering of the bilevel halftone image. Then we predict the reflectance spectra defined by the continuous-level models by fitting the bilevel models' effective ink surface coverages. Since dot blurring tends to increase the absorption of light by the ink, the effective ink surface coverage is larger than the nominal one, i.e., dot blurring induces its own contribution to dot gain. Dot blurring can also be accurately modeled by an increased n-value of the classical Yule–Nielsen model.

OCIS codes: 100.2810, 330.1710.

1. INTRODUCTION

Printed halftone colors are produced by depositing ink dots of variable size on paper. Accurate prediction of the printed halftone reflection spectra is difficult due to the occurrence of physical phenomena that depend on the printing process, the inks, and the print substrate. In order to predict the reflection spectrum of halftone prints, mathematical models have been developed relying on geometrical optics or on empirical formulas. The simplest model relies on the Murray–Davies equation (1) or on its version with reflectances instead of densities. A single-ink halftone is composed of two colorants: the inked paper (reflectance R_i and fractional area a) and the unprinted paper (reflectance R_p and fractional area $1-a$). The global reflectance of the print is given by the sum of the two colorant reflectances weighted by their respective fractional areas:

$$R(\lambda) = (1-a)R_p(\lambda) + aR_i(\lambda). \tag{1}$$

This model assumes that light does not propagate between the inked and non-inked areas. However, at middle and high screen frequencies, this assumption is not valid. Light is transferred between inked and non-inked areas due to scattering within the paper bulk and to multiple reflections between the paper bulk and the print–air interface. The relation between the global print reflectance and the colorant reflectances becomes nonlinear. Yule and Nielsen [2] modeled this nonlinearity by introducing a n factor into the Murray–Davies model. Viggiano [3] extended the Yule–Nielsen model to spectral predictions, yielding

$$R(\lambda) = [aR_i^{1/n}(\lambda) + (1-a)R_p^{1/n}(\lambda)]^n. \tag{2}$$

The n-value in the exponent depends on the printing device, the type of paper, and the halftone screen frequency. It is fitted from reflectance spectra measured on representative printed patches. According to Ruckdeschel and Hauser [4], the n-value should be contained between 1 and 2, but it is often larger [5] and may even be negative [6].

Clapper and Yule proposed a different reflectance model for halftone prints that describes the reflection of light in terms of attenuation by the ink, reflection by the paper substrate, and internal reflections at the print–air interface [7]:

$$R(\lambda) = T_{in}T_{ex}\frac{r_g(\lambda)[1-a+at(\lambda)]^2}{1-r_ir_g(\lambda)[1-a+at^2(\lambda)]}, \tag{3}$$

where T_{in} is the attenuation of the incident light due to the paper–air interface, T_{ex} the attenuation of the exiting light, r_i the internal reflectance of the paper–air interface [8,9], $r_g(\lambda)$ the intrinsic paper reflectance, a the ink surface coverage, and $t(\lambda)$ the ink transmittance. The intrinsic paper reflectance and the ink transmittance are deduced from the measured reflectances of the unprinted paper and of the solid ink print.

Due to lateral light scattering and multiple internal reflections, the ink dots appear larger than their physical size ("optical dot gain"). Moreover, mechanical phenomena occurring while depositing the inks yield irregular dot shapes, larger than expected and nonuniformly thick ("mechanical dot gain") [10–12]. The Yule–Nielsen model as well as the Clapper–Yule model account for them by fitting an effective ink surface coverage from reflectance spectra measured on printed patches. The difference be-

tween effective and nominal surface coverages is used to quantify a dot gain [13,14]. This dot gain is mainly a mechanical dot gain. However, since the prediction models do not completely account for the optical dot gain, a small part of the dot gain may also be due to optical phenomena.

Halftone print reflectance models were refined by focusing on the different phenomena contributing to dot gain, especially the diffusing properties of the paper [15–17] and the penetration of the inks into the paper [18,19]. Arney and Yamaguchi accounted for the ink thickness variation at the dot edges by introducing in their extended Murray–Davies model an additional empirically fitted parameter modifying the ink transmittance as a function of the dot surface coverage [5]. However, none of these contributions analyze the specific effect of dot blurring on halftone reflectance.

In the present work, we propose a theoretical study of halftone prints where the ink dots have a smooth, continuous thickness profile. We are interested in verifying to which extent the classical Clapper–Yule and Yule–Nielsen models are able to accurately predict their reflectance. In order to discard other phenomena such as the influence of one ink halftone on a second ink halftone, we consider only single-ink halftones. The single-ink halftone prints are simulated by specifying the spatial ink thickness distribution with a mathematical "halftone function." The reflectance of the variable ink thickness halftone print is calculated thanks to a spectral continuous-level prediction model. The smooth edge halftones are obtained by applying a Gaussian filter to the bilevel halftone, yielding a continuous-level halftone (Section 2). Since the ink thickness differs at each point, we adapt the notion of colorant present in the Yule–Nielsen and Clapper–Yule models by considering infinitesimal surface coverages and ink transmittances derived from the solid ink transmittance according to the position-dependent ink thickness (Section 3). With this extended colorant concept, we develop continuous versions of the Clapper–Yule and Yule–Nielsen models that enable the prediction of blurred halftone print reflectances (Section 4). We then verify to what extent the same reflectances can be predicted by the classical bilevel Clapper–Yule and Yule–Nielsen models by fitting effective ink surface coverages. The variation of the effective ink surface coverage is studied as a function of the blurring level in Section 5. We draw the conclusions in Section 6.

2. HALFTONE FUNCTION

A halftone print is obtained by depositing inks according to precomputed dot screens. The ink dots cover a certain fractional area a, called the ink surface coverage. Throughout our study, we assume uniform-intensity halftone patches, where the ink dots are all similar, circular, and located on a periodic grid, i.e., centered on points of integer coordinates.

The halftone layout is represented by a "halftone function" $F(x,y)$ specifying the ink thickness at each point (x,y). This function is the periodic repetition, of period 1, of a "dot function" f describing the bidimensional ink thickness profile of a single dot:

$$F(x,y) = \sum_i \sum_j f(x-i, y-j). \tag{4}$$

In the case of a bilevel halftone, the ink thickness is either 0 or 1. For an ink surface coverage a, the ink dots are disks of radius $\sqrt{a/\pi}$. The corresponding bilevel dot function f_0 represents the disk centered on the origin (0,0):

$$f_0(x,y) = \begin{cases} 1 & \text{if } \sqrt{x^2+y^2} < \sqrt{a/\pi} \\ 0 & \text{else} \end{cases}. \tag{5}$$

To avoid the case where the dots meet each other, we restrict our study to dot radii less than 1/2, i.e., to ink surface coverages less than $\pi/4 \asymp 0.78$.

We call "continuous-level halftone" a halftone whose ink thickness varies continuously over the surface. We develop the special case of "blurred halftones," whose dot function is obtained by blurring the bilevel dot function f_0. Blurring is performed by convolving f_0 with the Gaussian function parameterized by a "blurring coefficient" σ:

$$g_\sigma(x,y) = \frac{1}{2\pi\sigma^2} \exp\left(-\frac{x^2+y^2}{2\sigma^2}\right). \tag{6}$$

The blurred dot function is given by

$$f_\sigma(x,y) = \int_{-\infty}^{\infty} \int_{-\infty}^{\infty} f_0(u,v) g_\sigma(x-u, y-v) du dv, \tag{7}$$

and the blurred halftone function F_σ is obtained by repeating periodically f_σ according to Eq. (4). Taking advantage of the periodicity of the halftone function, one can reduce its definition domain to the unit square, i.e., $0 \leqslant x \leqslant 1$ and $0 \leqslant y \leqslant 1$. This domain intercepts only the four dots centered on the vertices (0,0), (0,1), (1,0), and (1,1). The defining expression for F_σ becomes

$$F_\sigma(x,y) = f_\sigma(x,y) + f_\sigma(x-1,y) + f_\sigma(x,y-1) + f_\sigma(x-1,y-1). \tag{8}$$

Although the bilevel halftone dots are disjoint, the blurred ink dots overlap each other beyond a certain blurring level. Thanks to the sums in Eqs. (4) and (8), the halftone function accounts for this overlap. Blurring modifies the ink thickness distribution but not the ink volume, expressed as the integral of the dot function over the considered surface. Since the Gaussian function g_σ satisfies the relation

$$\int_{-\infty}^{\infty} \int_{-\infty}^{\infty} g_\sigma(x,y) dx dy = 1, \tag{9}$$

the ink volume remains constant both within the dot function $f_\sigma(x,y)$ and within the halftone function $F_\sigma(x,y)$. Figure 1 shows examples of blurred halftones for an ink surface coverage of 0.6 and various blurring coefficients.

3. COLORANTS IN A CONTINUOUS-LEVEL HALFTONE

A halftone print is composed of small juxtaposed areas of uniform color, called "colorant areas" or simply "colorants." A colorant is either a layer of one ink with a given thickness or a superposition of different inks with given

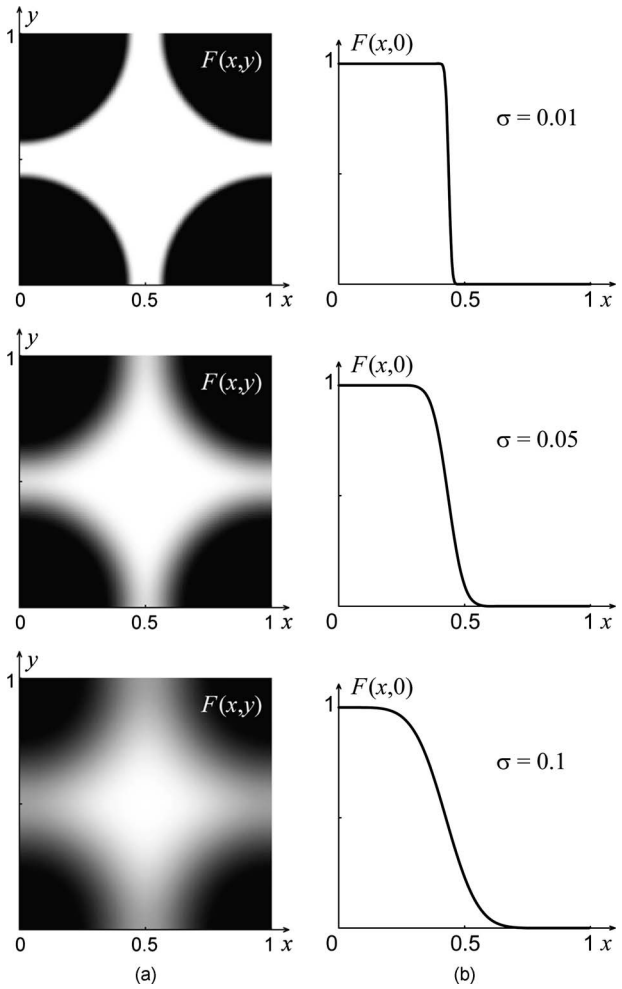

Fig. 1. (a) Blurred halftone function $F(x,y)$ for a surface coverage $a=0.6$ and various blurring coefficients σ and (b) the ink thickness of a single dot along the x axis.

thicknesses. From a given set of inks, one can obtain many different colorants by varying the thickness of the inks and/or superposing them.

Let us denote as $R_i(\lambda)$ the reflectance of a given printed colorant. The unprinted paper is also a colorant, whose reflectance is denoted as $R_p(\lambda)$. From the reflectances $R_i(\lambda)$ and $R_p(\lambda)$, which can be measured, we can deduce according to the selected spectral prediction model a transmittance $t(\lambda)$ representing the attenuation of light due to the ink layer. The unprinted paper is characterized by a colorant transmittance equal to 1.

A bilevel halftone contains two colorants corresponding to the paper areas with and without ink. In a continuous-level halftone, the ink thickness varies continuously over the print's surface. There is therefore a different colorant at each point. We associate with each colorant an infinitesimal surface coverage $dxdy$, as well as a transmittance $T(x,y)$ depending on the ink thickness specified by the halftone function $F(x,y)$,

$$T(x,y) = t^{F(x,y)}, \tag{10}$$

where t is the ink transmittance in the full coverage patch. Let us now relate this ink transmittance $t(\lambda)$ to the measured reflectance spectra according to the two classical reflectance prediction models: the spectrally extended Yule–Nielsen model [3] and the Clapper–Yule model [7].

A. Ink Transmittance in the Yule–Nielsen Model

With respect to the spectral Yule–Nielsen model, we assume that the attenuation due to the ink is given by the ratio of the solid ink print reflectance to the unprinted paper reflectance. Since the reflected light travels a double path across the ink, the solid ink print reflectance may be expressed as

$$R_i(\lambda) = R_p(\lambda) t_{yn}^2(\lambda). \tag{11}$$

When the ink thickness is γ, the solid ink print reflectance becomes

$$R_i^{(\gamma)}(\lambda) = R_p(\lambda) t_{yn}^{2\gamma}(\lambda) = R_p(\lambda) \left[\frac{R_i(\lambda)}{R_p(\lambda)} \right]^{\gamma}. \tag{12}$$

B. Ink transmittance in the Clapper–Yule model

According to the Clapper–Yule model, light crosses the ink layer more than twice due to the multiple reflections between the paper and the print–air interface. The solid ink print reflectance is expressed as a function of the intrinsic paper reflectance $r_g(\lambda)$, the ink layer transmittance $t(\lambda)$, and the Fresnel terms T_{in}, T_{ex}, and r_i associated with the print–air interface:

$$R_i(\lambda) = \frac{T_{in} T_{ex} r_g(\lambda) t^2(\lambda)}{1 - r_i r_g(\lambda) t^2(\lambda)}. \tag{13}$$

T_{in} is the transmission factor for the incident light crossing the interface, T_{ex} is the transmission factor for the emerging light, and r_i is the internal reflectance of the interface for the diffuse light reflected by the paper. These terms depend on the refractive index of the paper as well as, regarding T_{in} and T_{ex}, the orientation of light, i.e., the measuring geometry. For the classical 45°:0° geometry and a typical refractive index of paper 1.5, we have $T_{in}=0.95$, $T_{ex}=0.43$, and $r_i=0.60$ [8,9].

When $t(\lambda)=1$, Eq. (13) expresses the unprinted paper reflectance. From this equation and from the measured paper reflectance $R_p(\lambda)$, one deduces the intrinsic paper reflectance:

$$r_g(\lambda) = \frac{R_p(\lambda)}{T_{in} T_{ex} + r_i R_p(\lambda)}. \tag{14}$$

The ink transmittance is deduced from Eq. (13) with the obtained intrinsic paper reflectance $r_g(\lambda)$ and the measured solid ink print reflectance $R_i(\lambda)$:

$$t(\lambda) = \sqrt{\frac{R_i(\lambda)}{r_g(\lambda)[T_{in} T_{ex} + r_i R_i(\lambda)]}}. \tag{15}$$

4. CONTINUOUS HALFTONE REFLECTANCE MODELS

The aim of a reflectance prediction model is to predict the reflectance of halftone prints as a function of the surface coverage of its colorants. In the case of multi-ink bilevel halftones, the colorants correspond to the different super-

positions of inks. A halftone of p inks thus contains 2^p colorants. We now consider the case of single-ink continuous halftones where, due to variations in the ink thicknesses, a multitude of colorants with infinitesimal surface coverage is formed. The equations of the Yule–Nielsen model and of the Clapper–Yule model are extended in order to predict the reflectance of halftones whose variable–thickness dots are made of such colorants.

A. Continuous Yule–Nielsen Model

The classical Yule–Nielsen equation expresses the reflectance of a print containing N colorants as a function of the individual reflectances R_k of the colorants and their respective surface coverages a_k for a given n-value:

$$R_{YN}(\lambda) = \left[\sum_{k=1}^{N} a_k R_k^{1/n}(\lambda) \right]^n. \tag{16}$$

In the case of single-ink continuous-level halftones, the relative ink thickness, given by the halftone function $F(x,y)$, varies at each point and forms a colorant continuum whose local reflectance is given by Eq. (12). Since all the colorants have the infinitesimal surface coverage $dxdy$, the sum in Eq. (16) becomes a double integral. We obtain for each wavelength the following reflectance expression called the "continuous Yule–Nielsen equation," whose n-value is denoted as n_c:

$$R_{YN} = R_p \left[\int_{x=0}^{1} \int_{y=0}^{1} (R_i/R_p)^{F(x,y)/n_c} dxdy \right]^{n_c}. \tag{17}$$

B. Continuous Clapper–Yule Model

The Clapper–Yule model expresses the reflectance of a halftone print containing N colorants as

$$R_{CY}(\lambda) = \frac{T_{in} T_{ex} r_g(\lambda) \left[\sum_{k=1}^{N} a_k t_k(\lambda) \right]^2}{1 - r_i r_g(\lambda) \sum_{k=1}^{N} a_k t_k^2(\lambda)}, \tag{18}$$

where $t_k(\lambda)$ and a_k denote, respectively, the transmittance and the surface coverage of colorant k. The terms T_{in}, T_{ex}, and r_i have the same meaning as in Eq. (13).

For single-ink continuous-level halftones, the infinitesimal ink surface coverages $dxdy$ yield double integrals instead of discrete sums. The colorant transmittances are given by Eq. (10), where transmittance $t(\lambda)$ is deduced from the solid ink patch reflectance according to Eq. (15) and reflectance $r_g(\lambda)$ is deduced from the measured paper reflectance according to Eq. (14). We obtain for each wavelength the following reflectance expression, called "continuous Clapper–Yule equation":

$$R_{CY} = \frac{T_{in} T_{ex} r_g \left[\int_{x=0}^{1} \int_{y=0}^{1} t^{F(x,y)} dxdy \right]^2}{1 - r_i r_g \int_{x=0}^{1} \int_{y=0}^{1} t^{2F(x,y)} dxdy}. \tag{19}$$

C. Comparison between the Reflectances of Bilevel and Continuous-Level Halftones

Let us examine the effect of dot blurring on the resulting halftone reflectance through the example of cyan ink printed at 50% surface coverage. The measured spectra of the paper and of the solid ink patch used for the simulation are plotted in Figure 2. The reflectance $R(\lambda)$ of the bilevel halftone is calculated with the classical Clapper–Yule model according to Eq. (3). The blurred print reflectance $R_\sigma(\lambda)$ is calculated by the continuous Clapper–Yule equation according to Eq. (19) with a blurring coefficient $\sigma = 0.1$ and the halftone function $F_\sigma(x,y)$ obtained from Eqs. (6)–(8). The simulation shows that the blurred halftone print reflects less light than the bilevel one in the wavelength domain where the ink is absorbing. The CIELAB ΔE_{94} color difference between these two reflectance spectra is 1.50, therefore well perceptible by a human observer [20]. The continuous Yule–Nielsen model predicts a similar decrease of the reflectance. Since dot blurring tends to increase the absorption of light by the ink, it induces an additional dot gain.

5. DOT GAIN ANALYSIS

For a single printed ink, the classical Clapper–Yule and Yule–Nielsen models assume bilevel halftones, composed of two colorants. Their nominal surface coverages are assumed to be known, e.g., from the color separation stage. However, mechanical interactions between the ink and the paper modify the ink surface coverages and/or the ink thickness profile. In order to obtain accurate spectral reflectance predictions, effective surface coverages need to be known. With a given spectral prediction model, they can be fitted from measured reflectances of a few calibration patches, e.g., halftones printed at 0.25, 0.5, and 0.75 nominal surface coverages, by minimizing a distance metric between predicted and measured reflection spectra.

In order to analyze the dot gain induced by dot blurring, we simulate a blurred calibration patch of nominal surface coverage a and blurring coefficient σ. The continuous model calculates its reflectance $M(\lambda)$. The classical model predicts a reflectance $P_x(\lambda)$ for an ink surface coverage x. The x value for which $P_x(\lambda)$ is the closest to $M(\lambda)$ corresponds to the effective surface coverage of the calibration patch, denoted as a'. It is obtained by minimizing the sum of square differences between $M(\lambda)$ and $P_x(\lambda)$:

$$a' = \arg\min_x \sum_{\lambda=380}^{730} [P_x(\lambda) - M(\lambda)]^2. \tag{20}$$

From several calibration patches printed with different nominal surface coverages, we obtain first a list of effective surface coverages a' and then by linear interpolation a continuous curve $a' = f(a)$. The gain in ink surface coverage is given by the difference between the effective and the nominal surface coverages, i.e., $a' - a = f(a) - a$. This last function defines the "dot gain curve."

A. Dot Gain Analysis with the Clapper–Yule Model

Let us come back to the example of cyan halftone prints, using the same reflectance spectra for the paper and the

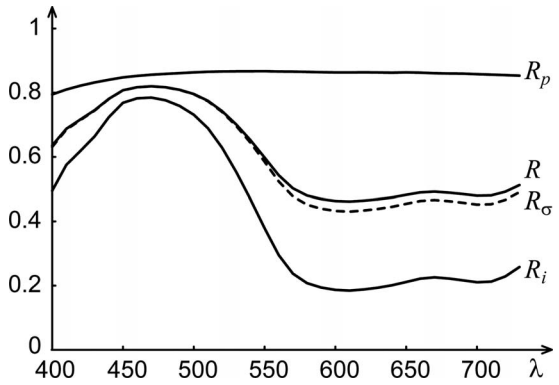

Fig. 2. Reflectances of the paper, R_p, of the solid cyan ink print, R_i, of a 50% bilevel halftone, R, and of the blurred halftone obtained with $\sigma=0.1$, R_σ. R_p and R_i are measured. R and R_σ are predicted by the classical and the continuous Clapper–Yule model, respectively..

solid cyan ink patch as in Fig. 2. The reflectance spectra $M(\lambda)$ of blurred halftone prints form the ground truth and are calculated by the continuous Clapper–Yule model for the blurring coefficients $\sigma=0.01$, 0.05, 0.1, 0.15, and 0.2 and for the ink surface coverages $a=0.05, 0.1, 0.15, \ldots, 0.75$. For each combination of blurring coefficient and ink surface coverage, an effective ink surface coverage a' is fitted according to Eq. (20) with the reflectance P_x given by the classical Clapper–Yule equation (3):

$$a' = \arg\min_x \sum_{\lambda=380}^{730} \left\{ \frac{T_{in}T_{ex}r_g(\lambda)[1-x+xt(\lambda)]^2}{1-r_ir_g(\lambda)[1-x+xt^2(\lambda)]} - M(\lambda) \right\}^2. \tag{21}$$

For each blurring coefficient, the obtained list of effective ink surface coverages yields a dot gain curve, plotted in Fig. 3. Since the halftone function is defined for ink surface coverages less than 0.78, the curves are extrapolated beyond $a=0.75$ by assuming that no dot gain occurs for solid ink.

As already noticed when analyzing Fig. 2, blurring increases the dot gain. It is interesting to observe that the ink surface coverage yielding the highest dot gain decreases as blurring increases. The ΔE_{94} values mentioned in the figure designate the CIELAB color difference between the reflectance $M(\lambda)$ calculated by the continuous model and the reflectance $P_{a'}(\lambda)$ predicted by the classical model at the fitted surface coverage a'. Only the largest color difference is mentioned, which coincides with the largest dot gain. The color difference becomes important for the highest blurring coefficients, e.g., $\sigma>0.1$. This means that the classical Clapper–Yule model has difficulties reproducing the spectrum defined by the continuous model, even with optimal effective ink surface coverages.

B. Dot Gain Analysis with the Yule–Nielsen Model

Let us now study the influence of dot blurring according to the Yule–Nielsen model. The reflectances $M(\lambda)$ of the different calibration patches form the ground truth and are calculated by the continuous Yule–Nielsen equation (17) with $n_c=3.5$. This typical n-value was inspired by previous work carried out with inkjet prints [13]. Then we use the bilevel Yule–Nielsen equation (2) and fit the effective surface coverages according to the minimization equation (20). The n-value n_b used in the bilevel Yule–Nielsen equation is the same as the one used in the continuous-level Yule–Nielsen equation, i.e., $n_b=n_c=3.5$:

$$a' = \arg\min_x \sum_{\lambda=380}^{730} \{[xR_i^{1/n_b}(\lambda) + (1-x)R_p^{1/n_b}(\lambda)]^{n_b} - M(\lambda)\}^2. \tag{22}$$

The dot gain curves predicted by the Yule–Nielsen model are similar to those predicted by the Clapper–Yule model, even though sensibly lower (Fig. 4). However, the Yule–Nielsen model has less difficulty than the Clapper–Yule model in reproducing the reflectance spectrum predicted by its continuous model. The largest color differences mentioned in Fig. 4 are lower than their equivalent ones in Fig. 3. Moreover, they are all inferior to 1, i.e., lower than the threshold of perception by human vision.

Lower dot gain curves are obtained when n_b is increased (see Appendix A). In order to find the optimal n_b

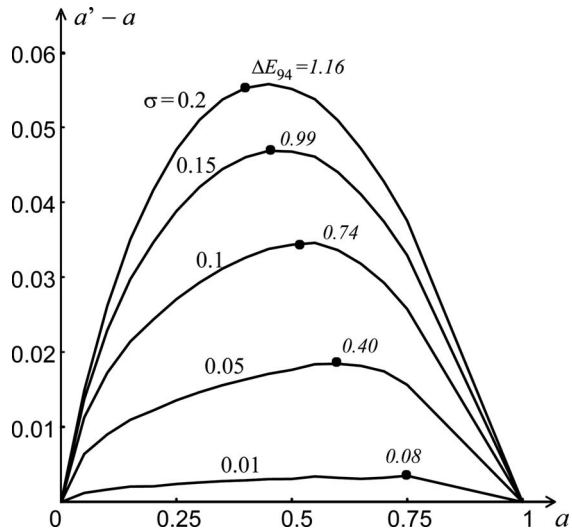

Fig. 3. Dot gain curves predicted by the Clapper–Yule model for various blurring coefficients.

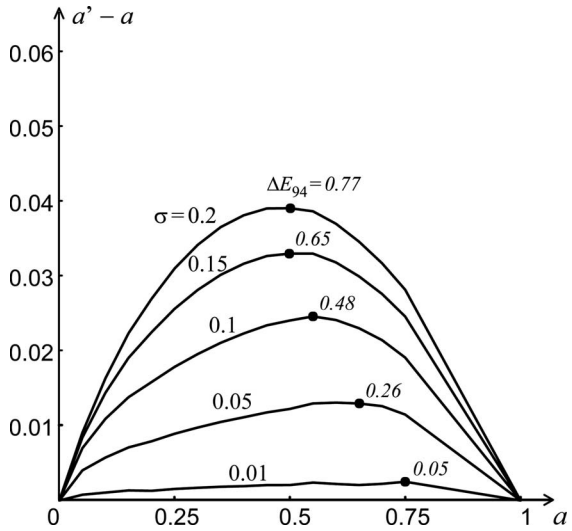

Fig. 4. Dot gain curves predicted by the Yule–Nielsen model for various blurring coefficients and for $n_b=n_c=3.5$.

and the optimal effective ink surface coverages yielding reflection spectra closest to the ones defined by the continuous model, we fit all the parameters simultaneously by a single minimization equation. The fitted n_b increases exponentially as the blurring coefficient increases, while the obtained dot gain curves are very close to zero. We obtain closely identical results by setting the dot gain curves to zero, i.e., by taking effective ink surface coverages equal to the nominal ones, and by fitting only the n_b-value (see Fig. 5). The fit of n_b relies on three reflectances M_k, simulated by the continuous Yule–Nielsen model with $n_c = 3.5$, corresponding to the three ink surface coverages $a_k = \{0.25, 0.5, 0.75\}$:

$$n_b = \arg\min_u \sum_k \left[\sum_{\lambda=380}^{730} \{[a_k R_i^{1/u}(\lambda) + (1 - a_k) R_p^{1/u}(\lambda)]^u - M_k(\lambda)\}^2 \right]. \quad (23)$$

For all the considered blurring coefficients and surface coverages, the reflectance spectrum predicted by the bilevel Yule–Nielsen model with fitted n_b is extremely close to the one simulated by the continuous model. The ΔE_{94} color differences are close to zero. An increase of n_b without modification of the ink surface coverage is therefore sufficient to perfectly model the effects of halftone dot blurring. According to this study, it seems preferable to predict the reflectance of blurred halftone prints with the Yule–Nielsen model rather than with the Clapper–Yule model.

Note that the experiments presented in this section were also carried out by selecting other values for the n_c-value used in the continuous Yule–Nielsen model when simulating the reflectance of the blurred halftone prints. The surface coverages fitted according to Eq. (22) and the n_b-value fitted according to Eq. (23) vary in a similar manner, as presented in Figs. 3 and 4. We also verified that the same results are obtained when using a magenta or yellow ink transmittance spectrum instead of a cyan ink transmittance spectrum.

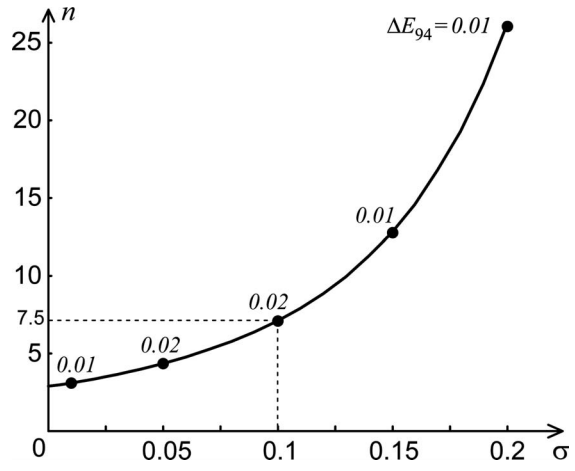

Fig. 5. Influence of the blurring coefficient on the n-factor fitted from three blurred halftone patches with ink surface coverages 0.25, 0.5, and 0.75 by considering the effective surface coverages equal to the nominal ones.

6. CONCLUSIONS

Two main contributions have been introduced. The first one is the extension of the Clapper–Yule and Yule–Nielsen spectral reflectance prediction models to single-ink continuous halftones, i.e., halftones with a continuous ink thickness profile. The extended models rely on a multitude of colorants whose transmittance depends on the ink thickness specified by a halftone function. Since the colorants are different at each point, their surface coverages are infinitesimal. Therefore, the sums in the Clapper–Yule and Yule–Nielsen equations become integrals. The second contribution is the use of the extended Clapper—Yule and Yule—Nielsen models to study the influence of ink dot blurring on the reflectance of halftone prints. Since it is not possible to ask a given printing device to produce different blurring levels, the extended models helped in simulating blurred halftone print reflectances. We could verify to what extent the classical Clapper–Yule and Yule–Nielsen models are able to predict the reflectance of blurred halftone prints by fitting effective surface coverages. The first observation is the fact that the fitted surface coverages increase with the blurring level. Therefore, dot blurring induces its own contribution to dot gain. With the fitted effective ink surface coverages, the classical Clapper–Yule model provides satisfying predictions despite a small loss of prediction accuracy when blurring becomes important. The predictions provided by the classical Yule–Nielsen model are more accurate, especially when fitting the Yule–Nielsen n-value instead of the ink surface coverages. The n-value increases with the dot blurring level and accounts perfectly for the dot blurring effect. This justifies the choice of a high n-value for prints having a blurred dot profile.

APPENDIX A: INFLUENCE OF THE YULE–NIELSEN *N*-VALUE ON DOT GAIN CURVES

For a given blurred halftone print, the reflectance calculated by the continuous Yule–Nielsen model is accurately predicted with the classical bilevel Yule–Nielsen model by fitting an effective ink surface coverage. When the two models use the same n-value, the fitted ink surface coverage is larger than the nominal one, i.e., the dot gain is positive (see Fig. 4). When the n_b-value of the classical Yule–Nielsen model is increased, lower effective ink surface coverages are obtained. Therefore, increasing the n_b-value reduces the computed dot gain. This is illustrated in Figs. 6 and 7 where the dot gain is computed from reflectances simulated with a blurring coefficient of 0.1 and with the same n-value $n_c = 3.5$ as in Section 5. The simulations rely on the same paper and same ink as in Figs. 2 and 4. Beyond a certain n_b-value, the dot gain becomes negative. The CIELAB ΔE_{94} color differences shown in italic in Fig. 7 indicate the color difference between the reflection spectra calculated by the continuous model and predicted by the bilevel model with various n_b-values. We observe that the matching is better when the dot gain becomes minimal (in absolute terms). Therefore, there exists an optimal n_b for which the bilevel Yule–Nielsen model yields spectral predictions nearly equiva-

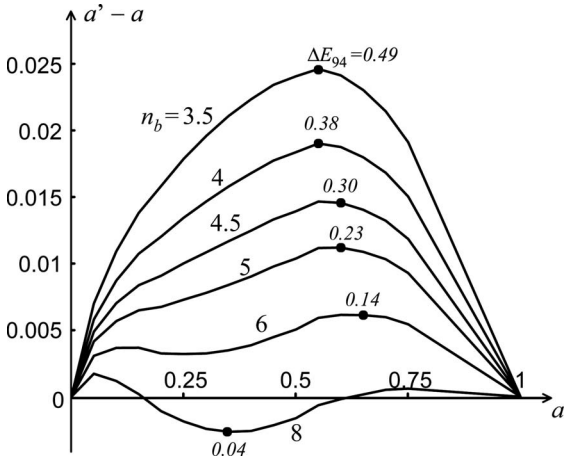

Fig. 6. Dot gain curves calculated using the bilevel Yule–Nielsen model with various n_b-values, from print reflectances simulated by the continuous-level Yule–Nielsen model with n_c =3.5 for a blurring coefficient σ=0.1.

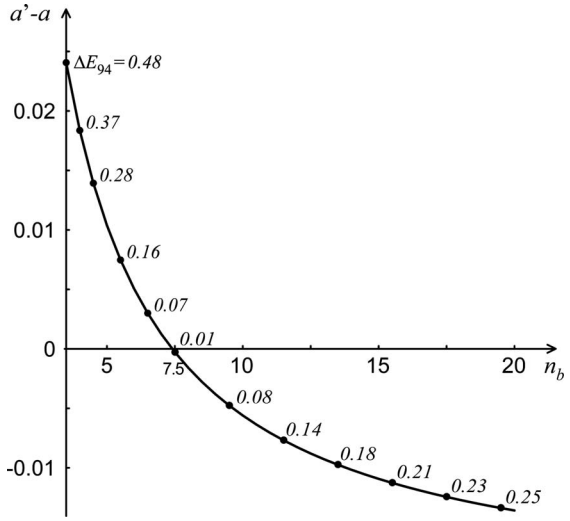

Fig. 7. Fitted optimal dot gain for the 0.5 surface coverage halftone with a blurring coefficient σ=0.1.

lent to the ones given by the continuous Yule–Nielsen model. Since this optimal n_b corresponds to the lowest dot gain, its variation as a function of the blurring coefficient is substantially the same as in Fig. 5, where a dot gain of zero was assumed. For a blurring coefficient σ=0.1, the optimal value n_b=7.5 can be read on both Figs. 5 and 7.

ACKNOWLEDGMENTS

The authors thank the Swiss National Foundation for their funding effort, grants 200020-105119and 200020-126757.

REFERENCES

1. A. Murray, "Monochrome reproduction in photoengraving," J. Franklin Inst. **221**, 721–744 (1936).
2. J. A. C. Yule and W. J. Nielsen, "The penetration of light into paper and its effect on halftone reproduction," in *Proceedings of TAGA* (Technical Association of the Graphic Arts, 1951), Vol. 3, 65–76.
3. J. A. S. Viggiano, "The color of halftone tints," *in Proceedings of TAGA* (Technical Association of the Graphic Arts, 1985), Vol. 37, pp. 647–661.
4. F. R. Ruckdeschel and O. G. Hauser, "Yule–Nielsen effect in printing: a physical analysis," Appl. Opt. **17**, 3376–3383 (1978).
5. J. Arney and S. Yamaguchi, "The physics behind the Yule–Nielsen equation," in *Proceedings of PICS 1999: Image Processing, Image Quality, Image Capture, Systems Conference* (Society for Imaging Science and Technology, 1999), pp. 381–385.
6. A. Lewandowski, M. Ludl, G. Byrne, and G. Dorffner, "Applying the Yule–Nielsen equation with negative *n*," J. Opt. Soc. Am. A **23**, 1827–1834 (2006).
7. F. R. Clapper and J. A. C. Yule, "The effect of multiple internal reflections on the densities of halftone prints on paper," J. Opt. Soc. Am. **43**, 600–603 (1953).
8. D. B. Judd, "Fresnel reflection of diffusely incident light," J. Res. Natl. Bur. Stand. **29**, 329–332 (1942).
9. M. Hébert and R. D. Hersch, "Classical print reflection models: a radiometric approach," J. Imaging Sci. Technol. **48**, 363–374 (2004).
10. K. Iino and R. Berns, "Building color management modules using linear optimization. I. Desktop color system," J. Imaging Sci. Technol. **42**, 79–94 (1998).
11. K. Iino and R. Berns, "Building color management modules using linear optimization. II. Prepress system for offset printing," J. Imaging Sci. Technol. **42**, 99–114 (1998).
12. R. Balasubramanian, "Optimization of the spectral Neugebauer model for printer characterization," J. Electron. Imaging **8**, 156–166 (1999).
13. P. Emmel and R. D. Hersch, "Modeling ink spreading for color prediction," J. Imaging Sci. Technol. **46**, 237–246 (2002).
14. R. D. Hersch, P. Emmel, F. Collaud, and F. Crété (2005), "Spectral reflection and dot surface prediction models for color halftone prints," J. Electron. Imaging **14**, 33001–12.
15. G. Rogers, "Optical dot gain in a halftone print," J. Imaging Sci. Technol. **41**, 643–656 (1997).
16. G. Rogers, "Optical dot gain: lateral scattering probabilities," J. Imaging Sci. Technol. **42**, 341–345 (1998).
17. J. S. Arney and M. L. Alber, "A probability description of the Yule–Nielsen effect I," J. Imaging Sci. Technol. **41**, 633–636 (1997).
18. J. S. Arney and M. L. Alber, "Optical effects of ink spread and penetration on halftones printed by thermal ink jet," J. Imaging Sci. Technol. **42**, 331–334 (1998).
19. L. Yang, R. Lenz, and B. Kruse, "Light scattering and ink penetration effects on tone reproduction," J. Opt. Soc. Am. A **18**, 360–366 (2001).
20. G. Sharma, "Color fundamentals for digital imaging," in *Digital Color Imaging Handbook*, G. Sharma, ed. (CRC Press, 2003), pp. 30–36.